Kinetics of Metal-Affinity Driven Self-Assembly between Proteins or Peptides and CdSe−ZnS Quantum Dots

Kim E. Sapsford,[†,||] Thomas Pons,[‡,#] Igor L. Medintz,[†] Seiichiro Higashiya,[§] Florence M. Brunel,[⊥] Philip E. Dawson,[⊥] and Hedi Mattoussi*[,‡]

Center for Bio/Molecular Science and Engineering, U.S. Naval Research Laboratory, Code 6900, Washington, D.C. 20375, Division of Optical Sciences, U.S. Naval Research Laboratory, Code 5611, Washington, D.C. 20375, Department of Chemistry, University of Albany-SUNY, 1400 Washington Avenue, Albany, New York 12222, and Departments of Cell Biology & Chemistry and the Skaggs Institute for Chemical Biology, The Scripps Research Institute, La Jolla, California 92037

Received: May 9, 2007

We present a molecular characterization of metal-affinity driven self-assembly between CdSe−ZnS core−shell quantum dots (QDs) and a series of proteins and peptides appended with various length polyhistidine tags. In particular, we investigated the kinetics of self-assembly between surface-immobilized QDs and proteins/peptides under flow conditions, as well as between freely diffusing QDs and proteins/peptides (solution phase). In the first configuration, QDs were immobilized onto functionalized substrates and then exposed to dye-labeled peptides/proteins. Using evanescent wave excitation, we assessed self-assembly by monitoring the time-dependent changes in the dye fluorescence. In solution, the kinetics of self-assembly was monitored via energy transfer between QDs and dye-labeled proteins/peptides. These measurements allowed determination of the kinetic parameters, including the association and dissociation rates (k_{on} and k_{off}) and the apparent binding constant (K_d). We find that self-assembly is rapid with an equilibrium constant $K_d^{-1} \approx 1$ nM for solution self-assembly, confirming that metal-affinity interactions provide QD bioconjugates that are functional and stable.

Introduction

A variety of strategies have been developed in the past few years for conjugating proteins, peptides, and oligonucleotides to semiconductor nanocrystals (quantum dots, QDs).[1,2] This has been motivated by the increasing interest in using luminescent QDs in biology, where applications such as immunoassays, nucleic acid detection, fluorescence resonance energy transfer (FRET)-based assays, tissue and cellular imaging, and single molecule monitoring can substantially benefit from their unique photophysical properties.[1−5] Conjugation methods reported to date include "covalent" attachment, usually via carbodiimide chemistry, use of biotin−avidin chemistry, direct capping with biologically active moieties such as peptides, as well as use of electrostatic interactions.[1,2,6] Many of these conjugation techniques, however, are multistep processes and further require careful purification of the final QD bioconjugates.[2]

We have developed an alternate conjugation strategy based on self-assembly driven by specific metal-affinity interactions between proteins or peptides appended with C- or N-terminal polyhistidine sequences (His_n tag) and hydrophilic CdSe−ZnS core−shell QDs. His_n sequences are commonly introduced into proteins or added into nascent peptide sequences to facilitate purification over immobilized metal-affinity chromatography (IMAC) media such as nickel−nitrilotriacetic acid (Ni−NTA) resin.[7,8] Assay results collected from self-assembled QD bioconjugates including photoluminescence increases, electrophoresis, and FRET indicate that conjugate formation is complete within 10−15 min of reagent mixing. They also indicate that control over conjugate valence can be exerted through the molar ratios of the QDs and His_n-appended biomolecules used.[9−12] We have, for example, utilized this conjugation process to self-assemble several hybrid QD protein/peptide sensors able to detect the presence of specific targets; these include the nutrient maltose, the explosive TNT, and several proteolytic enzymes.[10,11,13] This conjugation strategy has also been employed by other groups to probe interactions with cellular membranes, prepare fluoroimmunoreagents, and assemble photocatalytic cytochrome QD hybrids.[14−19]

Preliminary results indicate that QD−protein and QD−peptide conjugates formed using this rationale are stable to moderate changes in pH ($6 \leq pH \leq 10$) and temperature ($4 \leq T \leq 37$ °C).[13,14,20,21] It has, however, remained unclear whether the interactions between the His_n tag and QDs occur directly with the inorganic metal-rich surface or if they are mediated by electrostatic interactions with the surface ligands; nonetheless, electrostatically driven interactions have been proposed in ref 22. Furthermore, no investigation of the kinetics that drive QD−protein interactions has been carried out. Prior studies suggested that binding of His-tagged proteins to Ni ions immobilized onto gold nanoparticles via surface-attached NTA (where density of Ni^{2+} centers is higher) was improved compared with single-ion IMAC chelate media.[23] CdSe−ZnS QDs are very small in size but have large (metal-rich) surface-to-volume ratios. Thus,

* Corresponding author. E-mail: hedi.mattoussi@nrl.navy.mil.
[†] Center for Bio/Molecular Science and Engineering, U.S. Naval Research Laboratory.
[‡] Division of Optical Sciences, U.S. Naval Research Laboratory.
[§] University of Albany-SUNY.
[⊥] The Scripps Research Institute.
[||] Also, George Mason University, 10910 University Blvd., MS 4E3, Manassas, VA 20110.
[#] Present address: Ecole de Physique et Chimie Industrielle (ESPCI), Rue Vauquelin, 75005 Paris, France.

10.1021/jp073550t CCC: $37.00
Published on Web 07/19/2007

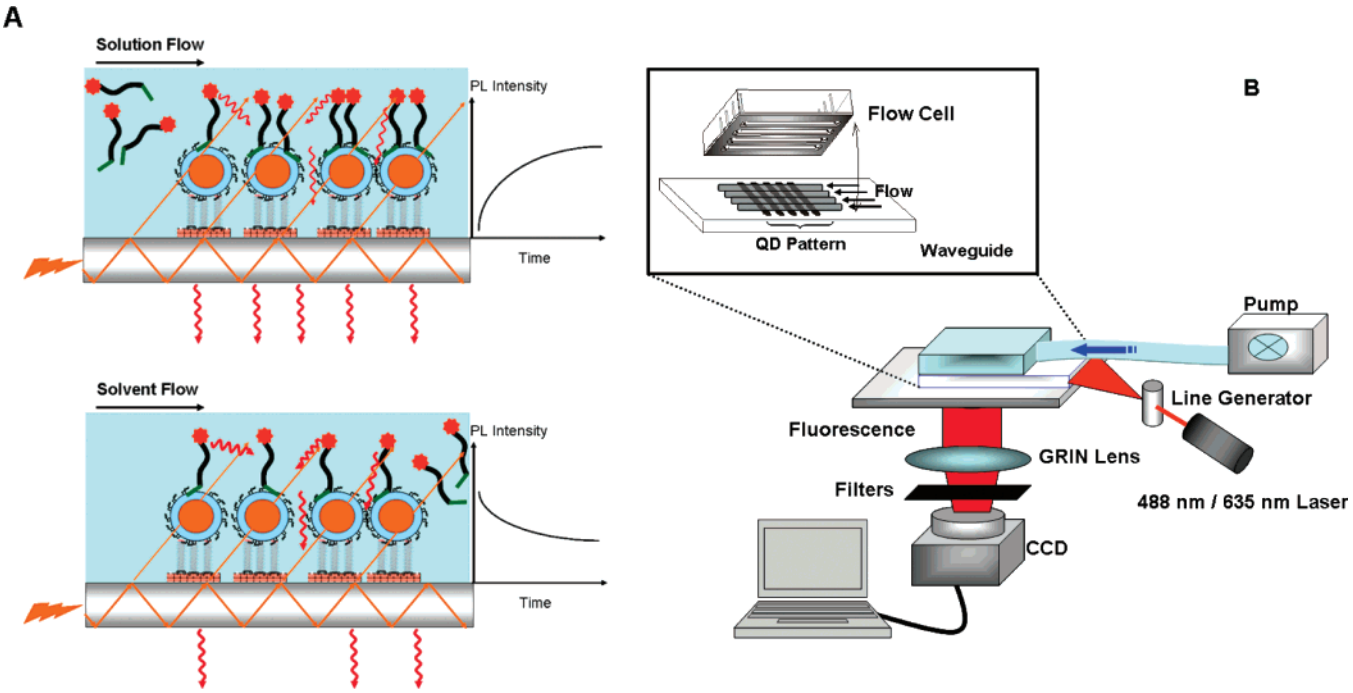

Figure 1. (A) Schematic representation of peptide surface self-assembly under applied flow (not to scale): Self-assembly buildup under solution flow (top) and slow dissociation of peptides under applied solvent flow (bottom). Evanescent wave excitation of the self-assembled QD−peptide conjugates through the substrate (which serves as a waveguide) along with signal collection (at right angle) are shown. (B) Schematics of the NRL array biosensor detection system used for fluorescent imaging of the surface self-assembled structures under continuous flow; a close-up of the array buildup is shown in the inset.

if polyhistidine tracts interact directly with the metal-rich surface, higher binding affinity should be expected for self-assembled QD−bioreceptor conjugates using His-appended proteins and peptides. To have better control over QD−protein/peptide conjugates formed using this method and to optimize their use in developing targeted biological applications, it is critical to develop a sound understanding of this conjugation strategy.

In this report, we evaluate the kinetics of metal-affinity driven self-assembly between CdSe−ZnS QDs and His-tagged proteins and peptides. We utilize a series of peptides and proteins functionalized with different polyhistidine lengths along with QDs capped with either charged dihydrolipoic acid (DHLA) or neutral poly(ethylene glycol)-appended DHLA (DHLA−PEG) ligands. Two particular configurations were explored: (1) self-assembly of proteins/peptides onto surface-immobilized QDs and (2) self-assembly between freely diffusing QDs and proteins/peptides in solutions. In configuration 1, QDs were first immobilized on the surface of glass substrates using heterobifunctional polypeptides, and then dye-labeled His_n-tagged proteins/peptides were continuously flowed over these surfaces to probe the real-time kinetics of protein-to-QD interactions. Capture of the peptide−dye/protein−dye by the QDs was monitored by measuring changes in the fluorescence from the dye, following direct excitation via an evanescent wave through the glass substrate (as schematically depicted in Figure 1). The resulting concentration and time-dependent changes in dye fluorescence intensity collected during self-assembly were used to derive kinetic parameters including the apparent association rate, k_{app}, the intrinsic association rate, k_{on}, the dissociation rate, k_{off}, and the apparent binding constant, K_d. Effects of His-tag length and pH of the buffer solution used were investigated. In solution (configuration 2), self-assembly was monitored by measuring changes in the rate of energy transfer between QDs and dye-labeled protein/peptide as a function of concentration and time. Estimates of the binding parameters were derived and compared to those extracted from surface self-assemblies.

Materials and Methods

Materials. CdSe−ZnS core−shell QDs with an emission maximum centered at 590 nm were synthesized using organometallic precursors reacted in a hot coordinating solvent mixture made of trioctyl phosphine and trioctyl phosphine oxide (TOP/TOPO) and amines, following the procedures described in refs 6 and 24−26. The nanocrystals were made hydrophilic by exchanging the native TOP/TOPO capping shell with DHLA, or DHLA-terminated with a poly(ethylene glycol) segment (MW $\approx$ 1000 Da), DHLA−PEG1000 ligands.[6,27]

The core synthetic peptide sequence used for testing self-assembly onto QDs consists of Ac-$(His)_n$GlyLeuAibAlaAlaGlyGlyHisTyrGlyCys-amide, where Ac is an acetyl group at the N-terminus, *n* designates repeats of either 2, 4, 6, or 8 histidine residues, and Aib is the noncoded residue α-amino isobutyric acid. Peptides were synthesized manually using in situ neutralization cycles for Boc solid-phase peptide synthesis.[28] All peptides used in this study have a free N-terminus. The peptide was monolabeled with an organic dye at the cysteine residue using monofunctional maleimide-Cy5 (GE Healthcare, Piscataway NJ), purified from unreacted dye using Ni−NTA agarose media (Qiagen, Valencia, CA), then dialyzed and desalted.[11,20] Labeling efficiency of the peptides was quantified using the absorption of the Cy5 dye. Additional details on peptide synthesis and purification are provided in the Supporting Information.

Maltose binding protein (MBP) was expressed in an *Escherichia coli* host strain and purified using Ni−NTA affinity chromatography.[29] Monofunctional maleimide-Cy5 was used to label the protein at a unique cysteine residue (95C) of the protein amino acid sequence.[10,12,29] MBP expressing either a C-terminal 5 or 11 histidine sequence (MBP-His_5 or MBP-His_{11}) was utilized. MBP-His_{11} differs from its MBP-His_5 precursor by the addition of a C-terminal Gly-Ser-$(His)_6$ sequence immediately following the original $(His)_5$ terminus as described in ref 21.

The $YEHK_5$ polypeptide (MW = 13.2 kDa) consists of the sequence Met-Gly-$(Cys)_2$-$(Gly)_4$-[$(Gly\text{-}Ala)_3$-Gly-Tyr-$(Gly\text{-}Ala)_3$-Gly-Glu-$(Gly\text{-}Ala)_3$-Gly-His-$(Gly\text{-}Ala)_3$-Gly-Lys]$_5$-Gly-Ala-$(His)_6$ with the core bracketed β-strand sequence repeated five times. After purification, the Cys residues were functionalized with EZ-link PEO-maleimide-biotin (Pierce Biotechnology, Rockford, IL). Additional details on the design, synthesis, labeling, and purification of this polypeptide are provided in ref 30.

Patterning of Quantum Dots onto NeutrAvidin-Functionalized Substrates. Microscope slides (which also serve as waveguides for evanescent wave excitation of the surface-immobilized QDs; Figure 1) were first functionalized with NeutrAvidin following a procedure previously described in refs 31 and 32. A six-channel patterning poly(dimethylsiloxane) (PDMS, Nusil Silicone Technology, Carpintera, CA) flow cell was attached to the surface of the NeutrAvidin slide (Figure 1). Biotin-functionalized $YEHK_5$-His_6 peptide diluted to 10 μg/mL in 10 mM sodium phosphate 150 mM NaCl 0.05% Tween-20 buffer at pH 7.4 (PBST buffer pH 7.4) was introduced into channels 2−6 and incubated overnight at 4 °C; channel 1 was exposed to buffer pH 7.4 (negative control). The flow cell was connected to a peristaltic pump, and the channels were rinsed with PBS buffer at a flow rate of 1.0 mL/min (~1 mL per channel). The waveguide was then exposed to the following solutions for 2 h at room temperature: channels 1 and 2 exposed to 10 mM borate buffer plus 0.05% Tween-20 pH 9.5 (BT buffer pH 9.5), and channels 3−6 incubated with 150 nM solution of QDs in Na−tetraborate buffer pH 9.5. The channels were then rinsed with 1 mL of buffer pH 9.5 at a flow rate of 0.4 mL/min, the PDMS flow cell was removed, and the patterned substrate was dried.

The above substrates were used to test the kinetics of metal-affinity interactions by exposing the immobilized QD arrays to solutions of dye-labeled His_n-appended peptides or proteins. For this, the slide was assembled with a second six-channel flow cell oriented at 90° with respect to the initial pattern (Figure 1B) and connected to an Ismatec peristaltic pump (Cole-Parmer Instrument Company, Chicago, IL) dispensing a continuous flow of Cy5-labeled protein (or peptide) solution into the flow channels. The second flow cell was machined in poly(methyl methacrylate) (Plexiglass G, Rohm and Haas, Philadelphia, PA) using a CNC mill and equipped with a black PDMS gasket to minimize background and light-scattering signals. This configuration provided an array of functionalized rectangles containing immobilized QDs that interact with flowing dye-labeled peptides and proteins under various conditions. The functionalized substrate/waveguide was placed on top of a slide holder, and the array was excited with an evanescent wave (Figure 1). Excitation was achieved using a 635-nm line provided by a 12 mW diode laser (Lasermax, Rochester, NY), focused into the end of the substrate/waveguide via a line generator placed before the sample. The latter ensured a homogeneous illumination throughout the glass substrate. Furthermore, using $\lambda_{exc} = 635$ nm (far from the absorption shoulder of the QDs) allowed exclusive excitation and monitoring of the dye fluorescence signal only as Cy5-peptide or Cy5-protein self-assembled onto the immobilized QDs. Solutions of Cy5-labeled peptide-His_n (~2−30 nM at either pH 7.4 or pH 9.5 conditions) or Cy5-labeled MBP-$His_{5,11}$ (1−400 nM at either pH 7.4 or pH 9.5 conditions) were then flowed through the channels at a rate of 0.72 mL/min. Fluorescence signal generated from the pattern (rectangles with captured peptide-Cy5) was collected at a right angle to the substrate using a GRIN lens array and imaged onto a Peltier-cooled CCD camera (Spectra Source, Teleris, Westlake Village, CA). A long-pass filter (Schott 0G-0665, Schott Glass, Duryea, PA) and a band-pass filter (Corion S40-670-S, Franklin, MA), placed before the camera, were also used to eliminate excitation and scattered signals. For on-flow kinetics, the image of the pattern was initially recorded at 10-s intervals, followed by longer time frames during a 20-min assembly monitoring period. The channels were then rinsed, with buffer only, at a flow rate of 0.72 mL/min, and off-flow or dissociation kinetics was monitored by measuring the time decay of the Cy5 PL signal. The configuration allowed at least four replicates to be tested for each concentration, with two control columns to assess effects of nonspecific interactions. No significant Cy5 photobleaching was observed in the time course of the experiment nor was any change in Cy5 PL in response to pH.

Analysis of the Fluorescence Images. A custom software application written in LabWindows/CVI (National Instruments, Austin, TX) was used to analyze the fluorescence images collected on the CCD camera. The software was used to generate a mask consisting of data rectangles enclosing the luminescent pattern, compared to background collected from the adjacent regions (dark rectangles located to the right and left of the fluorescent rectangles). For each slide, the fluorescence images collected for the various experimental conditions were analyzed in the order of collection. After analysis of the fluorescence signal for each condition, an Excel file was generated containing values of the mean intensity in each of the data rectangles, the mean intensity in each of the background rectangles, and the net intensity for each data rectangle (signal minus background) at each time increment. The data were further analyzed with SigmaPlot (Statistical Solutions, Saugus, MA) to extract the apparent time constants.

Monitoring of the Self-Assembly Kinetics in Solution. DHLA-capped or DHLA−PEG-capped QDs were dispersed in 10 mM Na−tetraborate buffer (pH 9.5) at concentrations ranging from 0.5 to 30 nM. Solutions were loaded in a 3-mL quartz cuvette, and a series of 1-s signal acquisitions at 590 nm (narrow window centered at the QD PL peak) were carried out using a SPEX Fluorolog-3 fluorimeter (Jobin Yvon/SPEX, Edison, NJ) and 350-nm excitation. Following an initial acquisition period from solution without any proteins present to ensure that QD PL signal was stable with time, Cy5-labeled proteins or peptides were added to the QD solution (at a protein-to-QD ratio of 1) and rapidly mixed, and PL acquisition was resumed. This allowed essentially continuous monitoring of the self-assembly kinetics. The 590-nm emitting QD-Cy5 donor−acceptor pair have a good spectral overlap (Supporting Information, Figure S-1), with a calculated Förster radius $R_0 = 60$ Å.[33] Binding of Cy5-labeled proteins (or peptides) to the QD surface leads to efficient FRET-driven quenching of the QD PL.[9] Here, we used this quenching to follow the kinetics of self-assembly with the His_n-tagged proteins/peptides. Dynamic FRET-driven quenching of the QD emission induced by collisions with free proteins was negligible in the nanomolar concentration range used. Apparent binding rates and the PL drop at self-assembly equilibrium were then derived from the PL decrease over time.

Analysis of the Binding Kinetics under Continuous Flow. We apply a first-order bimolecular reaction analysis to assess the kinetics of protein and peptide self-assembly on the QD surfaces, represented by:[32,34]

$$BS + P \rightleftharpoons BP \tag{1}$$

In eq 1, BS, P, and BP designate an available binding site on the surface of a QD, a free (unbound) protein/peptide, and a

protein/peptide bound to the QD, respectively. We define k_{on} and k_{off} as the intrinsic association (binding) and dissociation rates, respectively. Under sustained solution flow, the free protein/peptide concentration is determined by that of the reservoir solution and stays at $[P]_0$. Within the framework of a first-order bimolecular reaction model, the concentration of bound protein/peptide to the QD functionalized surface thus follows an exponential increase with time:[32,34]

$$[BP](t) \approx [P]_0(1 - \exp^{-k_{app}t}) \quad \text{with } k_{app} = k_{on}[P]_0 + k_{off} \tag{2}$$

where k_{app} is the apparent binding rate. When continuous flow is applied (on-phase, $[P] = [P]_0$), we use the time-dependent evolution of the fluorescence signal (proportional to the concentration of bound peptide dye/protein dye) to derive a value for the apparent binding rate:

$$S_{on}(t) = S_{\infty}(1 - \exp^{-k_{app}t}) \tag{3}$$

where $S_{on}(t)$ is the measured Cy5 fluorescence signal as a function of time and S_{∞} is the signal generated at equilibrium (plateau value). Values for the k_{on} and k_{off} rates can be derived from analysis of the fluorescence data at a minimum of two different concentrations $[P]_0$ using eqs 2 and 3. Conversely, during the off phase (when only buffer is flowed through the channels), the protein concentration in the solution is reduced to zero ($[P]_0 = 0$). This will induce the dye-labeled proteins/peptides to progressively disassemble (or detach) from the QD surface and result in an exponential time-dependent decrease of surface-bound peptides/proteins. The collected fluorescence signal will decay to a background value at a k_{off} rate, also following an exponential form:

$$S_{off}(t) = \Delta S \times \exp^{-k_{off}t} \tag{4}$$

where ΔS designates the amplitude of the fluorescence drop. Values for k_{off} derived from the off-phase measurements (via eq 4) are then compared to those derived from the on-phase kinetics (via eq 3) for several protein concentrations $[P]_0$. The equilibrium concentration $1/K_d$ (inverse of the binding constant, which designates the concentration at which half of the available binding sites are occupied) is then derived from the k_{on} and k_{off} values using:

$$\frac{1}{K_d} = \frac{k_{off}}{k_{on}} \tag{5}$$

Analysis of the Binding Kinetics in Solution. For these experiments, we maintain a small and constant total ratio of one protein/peptide per QD. The self-assembled QD bioconjugates used here have inherent heterogeneities in their valence due to the nature of multivalent interaction sites on the QD surface, and the distribution in the number of biomolecules per QD conjugate follows a Poisson statistical model.[35,36] For the present solutions, where a ratio of one protein-dye-to-QD was used (low valence), this will imply that in a sample most QDs will bind to one or zero protein, while a smaller fraction will be self-assembled with two or three proteins/peptides. For MBP, saturation of the QD surface usually occurs at ratios exceeding 15 proteins per QD.[6] By using a small ratio, at equilibrium and far from saturation, we can assume that a first protein bound to a QD does not influence the binding of a second or a third to that same QD as described by:

$$QD{-}P_n + P \leftrightarrow QD{-}P_{n+1} \tag{6}$$

where $QD{-}P_n$ and $QD{-}P_{n+1}$ designate a QD bound to n and $n + 1$ proteins, respectively, and P refers to a free protein. With these small ratios, we also assume that the association (binding) and dissociation rates do not depend on n, so that the concentration of bound proteins follows a monoexponential decay to an equilibrium value. As the number of self-assembled QD-protein-Cy5 in the sample increases, the ensemble QD PL systematically decreases because of FRET interactions. By increasing the QD and protein concentrations in the solution (while maintaining a fixed ratio of 1), the kinetics of QD−protein and QD−peptide self-assembly becomes more rapid. We fit the time-dependent QD PL decay at each concentration to a relation similar to the one used above (eq 3):

$$S_{QD}(t) = S_{QD|_0} - \Delta S_{QD}[1 - \exp(-k_{app}t)] \tag{7}$$

where $S_{QD|0}$ is the initial QD PL level and ΔS_{QD} is the amplitude of the QD PL drop. The apparent binding rate is given by:

$$k_{app} = k_{on}[QD]_0 + k_{off} \tag{8}$$

where $[QD]_0$ is the total QD concentration. Similar to flow experiments, we derive k_{on} and k_{off} by measuring k_{app} at several different QD concentrations, while maintaining the protein-dye-to-QD ratio constant at $n = 1$. In addition, the relative QD PL drop upon protein binding, $\Delta S_{QD}/S_{QD|0}$, is proportional to the fraction of bound dye-labeled proteins, $[BP]/[P]_0$. Since the interactions of a QD with one, two, or three proteins are essentially independent events (eq 6), the equilibrium relation can be expressed as $K_d^{-1} = [QD]_0[P]/[BP]$. Further manipulation of this expression provides a relation between the relative QD PL drop and the total QD concentration (a saturation curve):

$$\frac{\Delta S_{QD}}{S_{QD|_0}} \propto \frac{[QD]_0}{K_d^{-1} + [QD]_0} \tag{9}$$

Plotting the experimental values for $\Delta S_{QD}/S_{QD|0}$ versus $[QD]_0$ therefore provides a measure for the binding constant K_d^{-1}, the concentration at which half the proteins are bound to QDs while the other half is free, or equivalently, the concentration at which the relative PL drop reaches half of its maximum value.

Results

Specific Immobilization of Quantum Dots onto Substrates. The polypeptides used for surface immobilizing the QDs have a few unique features that provide inherent stability to the QD arrays. Each peptide consists of a core monomeric β-sheet structure with tyrosine (Y), histidine (H), glutamic acid (E), and lysine (K) residues located at the turns, an N-terminal His_6 tract for interactions with the nanocrystal surface, and a C-terminal Cys_2 (Supporting Information, Figure S-2).[30,37] The charges on the glutamic acid (negative) and lysine (positive) residues provide stiffness to the antiparallel structure (rigid "rodlike") via salt bridge formation. The C-terminal cysteine residues are functionalized with maleimide-biotin groups, which may enhance the peptide affinity to the substrate, since each peptide could potentially interact with two NeutrAvidin binding sites on the surface. The bivalent interactions are expected to enhance an already strong avidin−biotin binding (with a reported $K_D \approx 10^{-15}$ M).[38] In addition, the rigid structure of the peptide combined with a clearly exposed His_6 promote a favorable

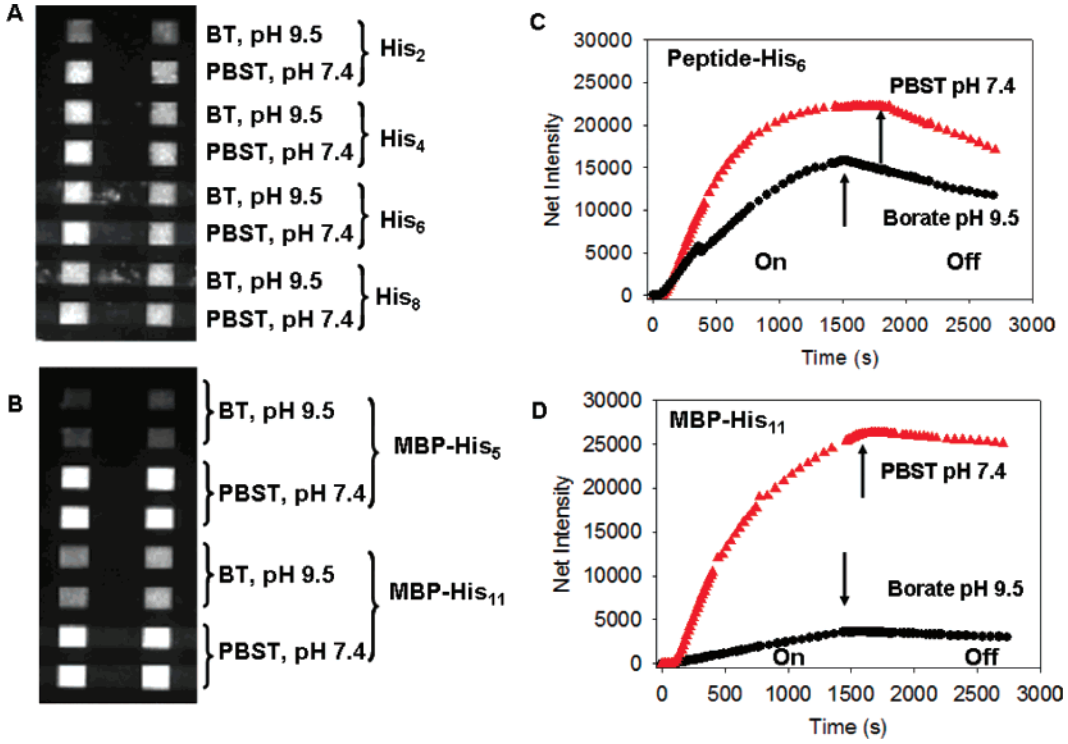

Figure 2. Effect of pH on the binding kinetics. (A) Fluorescence image collected using 635-nm excitation of a surface-immobilized QD layer incubated with ~40 nM Cy5-peptide-His_n (n = 2, 4, 6, or 8) in either pH 7.4 or pH 9.5 buffer followed by rinsing. (B) Fluorescence image of a QD layer exposed to 500 nM Cy5-MBP-$His_{5,11}$ in pH 7.4 or pH 9.5 buffer. (C and D) Plots of the net PL intensity versus time of a QD layer exposed to a continuous flow of solutions of 9.5 nM Cy5-peptide-His_6 (C) and 100 nM Cy5-MBP-His_{11} (D) at pH 7.4 or pH 9.5 buffer conditions. Arrows indicate the transition from on- to off-flow.

peptide orientation on the substrate and permit a single QD to interact with multiple $YEHK_5$, which stabilizes the QD array, as confirmed by the experimental results shown below. Initial experiments performed under static conditions (incubation with the appropriate solutions followed by rinsing) have shown that specific metal-affinity driven interactions mediate both immobilization of QDs onto the biotin-$YEHK_5$-His_6-functionalized substrate and subsequent capture of the Cy5-peptide-His (Supporting Information, Figure S-3). They also showed that nonspecific interactions were negligible.

Effects of pH on Peptide and Protein Self-Assembly on QD Arrays. Effects of pH on the stability of His-metal binding have been confirmed for a variety of systems. In particular, interactions of polyhistidine-appended proteins with Ni−NTA media are reported to be stable over the pH range 7−11 (basic conditions)[7,23,39] but become weaker in slightly acidic conditions (pH ≈ 6−7) and are fully disrupted at pH < 5, because of protonation of the imidazole side groups (histidine has a pK_a of 6 and remains charged (deprotonated) at neutral to basic conditions, pH ≥ 7).[7,23]

To assess the effects of solution pH conditions on the interactions between QDs and His-tagged proteins and peptides, we investigated the self-assembly of several Cy5-peptide-His_n (n = 2, 4, 6, 8) and Cy5-MBP-$His_{5,11}$, dispersed in buffer at either pH 7.4 (PBST) or pH 9.5 (BT), onto surface-immobilized QDs under static conditions. PBST at pH 7.4 is a physiologically relevant buffer commonly used in biology, and borate buffer is recommended for use with commercial QDs (http://www.invitrogen.com). The small amount of Tween-20 we added to our solutions serves to reduce nonspecific interactions during self-assembly.[31]

We compared the fluorescence intensities of the arrays collected after 20-min incubation with different solutions of Cy5-peptide-His_n and Cy5-MBP-$His_{5,11}$, followed by rinsing. Images shown in Figure 2A,B indicate that there are small changes in the fluorescence intensity measured at both pH's for Cy5-peptide-His_n sequences, with the exception of the Cy5-peptide-His_2, where a much stronger fluorescence intensity was measured at pH 7.4. In contrast, the effects of pH changes are more drastic on the capture of MBP-His where substantially lower fluorescence signals were measured at pH 9.5, indicating a lower concentration of self-assembled dye-labeled proteins. Furthermore, the difference was more pronounced for MBP appended with the shorter His_5 tag.

These observations were further tested by studying the kinetics of self-assembly to QD arrays under flow conditions using peptides and proteins dispersed in the two buffers. Figure 2C,D shows typical time-dependent intensity curves obtained for Cy5-peptide-His_6 and for MBP-His_{11} at pH 7.4 and pH 9.5 under on- and off-flow conditions. In both cases, data show higher density of surface assembly and faster binding kinetics in solution at pH 7.4 relative to those at pH 9.5 under flow conditions. The difference was, however, substantially more pronounced for self-assembly of MBP-His, where no time-dependent data could be collected for MBP-His_5 because of the rather low fluorescence signal. These results clearly complement the static binding data above where pronounced differences were measured primarily for self-assembly of MBP-His_n.

On the basis of these findings, we opted to investigate the kinetics of surface and solution self-assembly of the Cy5-peptide-His_n series using primarily solutions at pH 9.5. In comparison, surface self-assembly of MBP-$His_{5,11}$ was carried out in pH 7.4 and pH 9.5 buffers, while solution self-assembly was carried out using buffer at pH 9.5. This allowed us to explore all possible conditions and scenarios for QD−protein and QD−peptide self-assembly and to test the subtle effects of pH on surface (constrained interactions) versus solution self-assembly (freely diffusing QDs and proteins). The use of both

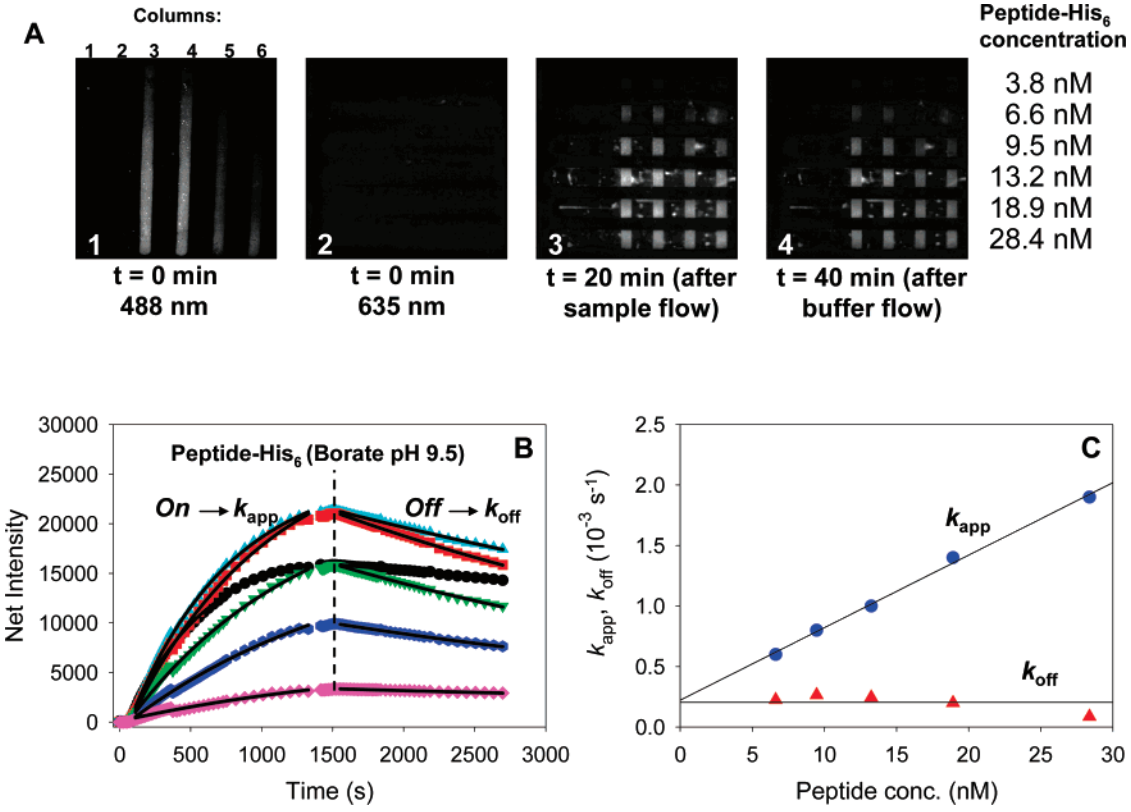

Figure 3. Kinetics of peptide self-assembly onto immobilized QDs. (A) Representative fluorescence images collected during the various steps of self-assembly as described in the text. Images 1 and 2 are collected at $t = 0$. (B) Plot of the net Cy5 PL intensity vs time for each Cy5-peptide-His_6 concentration fitted to monoexponential increase (on-flow) and decay (off-flow). The dashed line designates the change from on- to off-flow conditions. (C) Plot of the apparent binding rates k_{app} vs peptide concentration derived from the on-flow phase (●) together with the dissociation rates k_{off} (▲) derived from the off-flow phase.

peptides and proteins also allowed us to investigate the effects of the overall bioreceptor dimensions (4−4.5 kDa peptides versus full size 44−45 kDa proteins).

Kinetics of Peptide Self-Assembly onto Surface-Immobilized Quantum Dots. Figure 3A shows four representative fluorescence images collected from a QD array during exposure to increasing concentrations of Cy5-peptide-His_6 in BT buffer at different sequential elapsed times: at time $t = 0$ just before exposure (images 1 and 2), after 20-min exposure to sample flow (on-flow, image 3), and following 20-min exposure to buffer-only flow (off-flow, 40-min total elapsed time, image 4). Image 1 was collected using 488-nm excitation, whereas images 2, 3, and 4 were generated using 635-nm excitation. Image 1 clearly indicates successful surface immobilization of the 590-nm emitting QDs, while the lack of fluorescence signal in image 2 is due to absence of Cy5 emission (prior to exposure to Cy5-peptide solution and the negligible QD absorption at 635 nm). Images 3 and 4 indicate that Cy5 fluorescence signal was measured only in regions of immobilized QDs that were exposed to Cy5-peptide-His_6 solutions (columns 3−6). Furthermore, the change in fluorescence intensity was found to be concentration-dependent. In comparison, control columns 1 and 2, which were exposed to buffer only and a solution of biotin-$YEHK_5$-His_6 (without QDs), respectively, did not generate any signal (images 1−4, Figure 3A). Image 4 shows that after 20 min of exposure to buffer flow a slight decrease in the signal was recorded indicating that a partial dissociation or detachment of the Cy5-peptide-His_6 from the surface-immobilized QDs took place.

The fluorescence images were analyzed, and the net intensity (average in each row of squares) was plotted as a function of the elapsed time increments for the six different Cy5-peptide-His_6 concentrations for either on-flow or off-flow conditions (data are summarized in Figure 3B). The intensity data exhibited monoexponential behavior with time throughout each of the 20-min windows, in agreement with eq 3 (for on-flow) and eq 4 (for off-flow); values for k_{app} and k_{off} were extracted for each peptide concentration. Plots of these parameters vs peptide concentration (Figure 3C) clearly demonstrate that while k_{app} has a linear dependence on peptide concentration k_{off} stayed constant, in agreement with the prediction of eq 2. Data on fluorescence intensity vs time collected for each of the peptides appended with the various polyhistidine lengths showed similar behavior. A summary of the k_{app}, k_{off}, and $1/K_d$ values determined for each peptide-His_n is provided in Table 1. Overall, values for k_{on}, k_{off}, and $1/K_d$ were comparable for peptides appended with His_{4-8} tags. For the peptide appended with the shorter tag (His_2), smaller k_{on}, larger k_{off}, and higher equilibrium constant $1/K_d$ were measured. We should emphasize that at pH 7.4 the kinetics of self-assembly of His_6-terminated peptides was faster and the values measured for the $1/K_d$ were overall smaller (Table 1), as anticipated from the data shown in Figure 3.

We considered the possibility that, under continuous flow conditions used in this study, the QDs themselves may dissociate from the underlying biotin-$YEHK_5$-His_6 layer. However, fluorescence images of the QDs (using 488-nm excitation), taken before and after the assay was complete, consistently showed that only small to negligible changes in the QD PL were measured (Supporting Information, Figure S-4). The small decrease in QD PL could be attributed to FRET interactions between QDs and bound peptide-Cy5 because of favorable spectral overlap of this donor−acceptor pair. These findings clearly indicate that the QD layer adheres strongly to the

TABLE 1: Kinetic Parameters of Polyhistidine-Based Self-Assembly to QDs[a]

protein/peptide	buffer	estimated net charge	k_{on} (10^4 M^{-1} s^{-1})	k_{off} (10^{-4} s^{-1})	$1/K_d$ (nM)
		Determined under Continuous Flow			
peptide-His_2	borate pH 9.5	−2.1 (pH 7.4 + 0.1)	2.2 ± 0.1	10 ± 3	47 ± 11
peptide-His_4	borate pH 9.5	−2.1 (pH 7.4 + 0.3)	7.4 ± 0.3	1.4 ± 0.5	1.9 ± 0.7
peptide-His_6	borate pH 9.5	−2.1	6 ± 0.2	2.2 ± 0.3	3.7 ± 0.5
peptide-His_8	borate pH 9.5	−2.1 (pH 7.4 + 0.7)	4.8 ± 0.6	3.1 ± 0.7	6.5 ± 1.7
peptide-His_6	PBST pH 7.4	+0.5	16.5 ± 1.4	2.8 ± 0.3	1.7 ± 0.2
MBP-His_5	PBST pH 7.4	−4.4	6.0 ± 1.0	2.3 ± 0.6	3.8 ± 1.1
MBP-His_{11}	PBST pH 7.4	−3.7	2.9 ± 0.6	1.4 ± 0.3	5.0 ± 1.3
MBP-His_5[b]	borate pH 9.5	−18.5	NA	NA	NA
MBP-His_{11}	borate pH 9.5	−18.5	0.1 ± 0.01	1.2 ± 0.3	98 ± 27
		Determined from Solution-Phase FRET			
		Self-assembly onto DHLA-capped QDs			
MBP-His_5	borate pH 9.5	−18.5	NA	<30	0.7 ± 0.1
MBP-His_{11}	borate pH 9.5	−18.5	NA	<20	<0.5
peptide-His_6	borate pH 9.5	−2.1	350 ± 30	73 ± 17	2.1 ± 0.7
		Self-assembly onto DHLA−PEG1000-capped QDs			
peptide-His_6	borate pH 9.5	−2.1	NA	NA	<0.5

[a] Each value is the average of at least 4−6 replicates. NA: Not applicable. Net charge determined using protein calculator (http://molbiol-tools.ca). [b] No significant assembly noted under flow, see Figure 4.

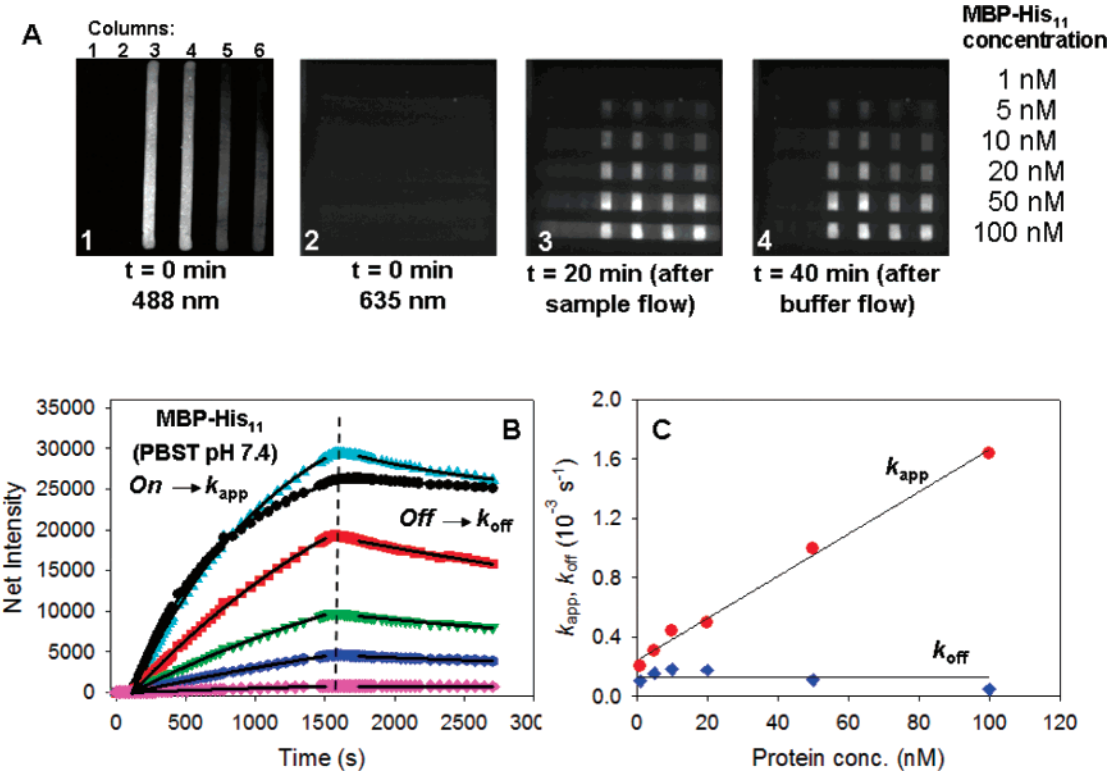

Figure 4. Kinetics of protein self-assembly onto immobilized QDs. (A) Selection of representative fluorescence images collected during the various steps as described in the text. (B) Plot of the net fluorescence intensity versus time for several concentrations of Cy5-MBP-His_{11} in PBST buffer fitted to monoexponential increases for on-flow and monoexponential decays for off-flow. The dashed line indicates change from on- to off-flow. (C) Plot of k_{app} and k_{off} versus protein concentration, derived from the on- and off-flow phases, respectively.

substrate. This is attributed to the multivalent interactions of the QDs with the underlying $YEHK_5$ peptide layer, combined with the strong anchoring of these capture peptides to the NeutrAvidin, as anticipated above.

Kinetics of Protein Self-Assembly onto Surface-Immobilized Quantum Dots. The above results using peptides were complemented with an investigation of the kinetics of protein self-assembly onto surface-immobilized QDs. Proteins are larger than peptides, and their overall charge may vary with the solution conditions. Studying their kinetics should provide additional insight into understanding the metal-His driven interactions with our QDs. Figure 4 shows typical fluorescence images collected from the surface arrays of QDs exposed to solutions of Cy5-MBP-His_{11} at several elapsed times. Images 1 and 2 were collected from a QD array prior to exposure to the protein solution and excited at 488 and 635 nm, respectively. Fluorescence images were also collected using 635-nm excitation following 20-min exposure of the QD array to a steady flow of protein solution (image 3 in Figure 4A, on-flow), then after an additional 20-min exposure to buffer-only flow (image 4 in Figure 4A, off-flow). As with the peptide experiments, before slide exposure to protein solutions, QD fluorescence was measured only when the system was excited at 488 nm (columns 2−6 in image 1), but no emission was recorded under 635-nm

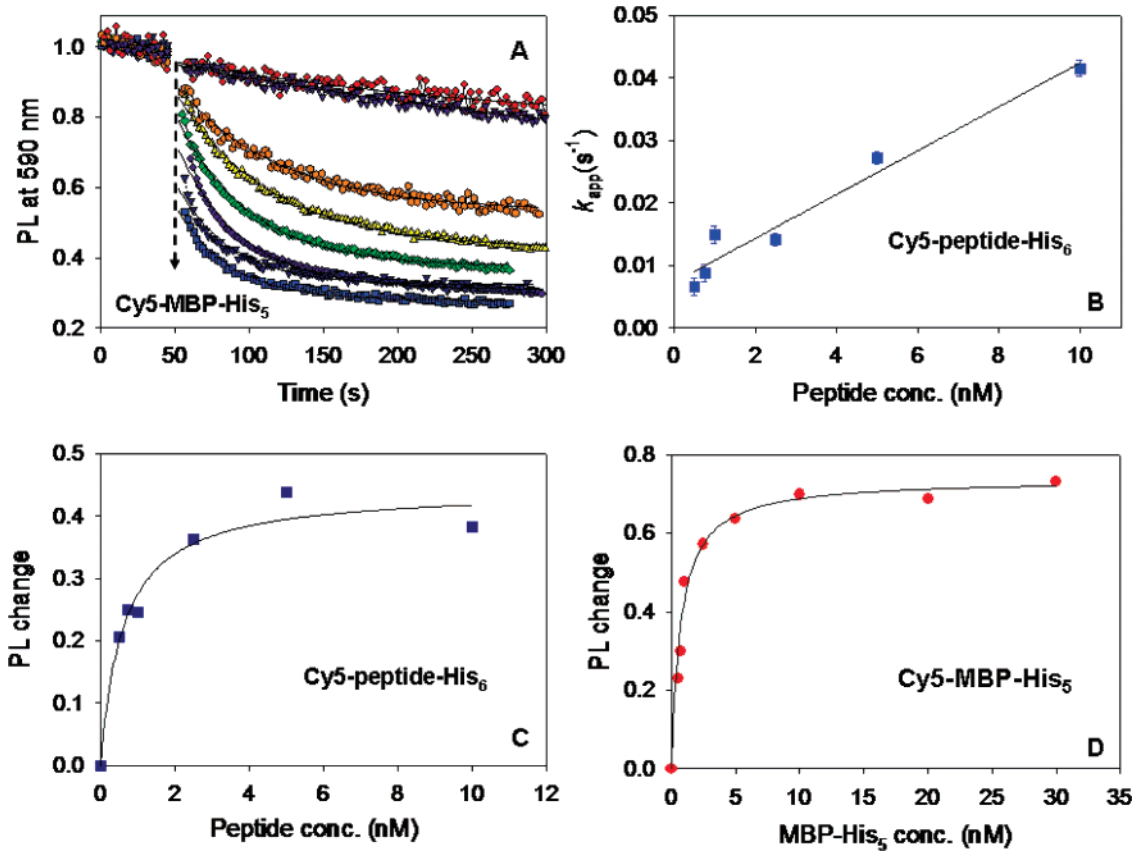

Figure 5. (A) Representative time traces of a 590-nm QD PL after mixing with Cy5-MBP-His_5 (arrow at $t \approx 50$ s points to increasing QD/protein concentration), normalized to its initial level at $t = 0$. The QD concentration was varied from 0.5 to 20 nM, and the amount of added proteins corresponded to a protein-to-QD ratio of 1. (B) Apparent binding rate vs concentration for Cy5-peptide-His_6 self-assembly onto 590-nm QDs. (C) Concentration-dependent relative PL loss of 590-nm QDs upon binding with Cy5-peptide-His_6 (peptide-to-QD ratio = 1). (D) Concentration-dependent relative PL change of 590-nm QDs upon binding with Cy5-MBP-His_5.

excitation (image 2), an expected result since no Cy5-MBP-His_{11} was present. In image 3, Cy5 signal was measured only in the QD-patterned regions of the waveguide that have been exposed to Cy5-MBP-His_{11} (see columns 3−6). After exposure to buffer-only solution, a decrease in the measured fluorescence signal was observed, which we attribute to partial dissociation of Cy5-MBP-His_{11} from the surface-tethered QDs (image 4). Again, the time-dependent changes in fluorescence intensity measured from images 3 and 4 were found to be concentration-dependent (compare rows 1 through 6, and corresponding plots in Figure 4B). Similar to what was recorded with the peptide series, the fluorescence intensity exhibited monoexponential dependence on time. Analysis of the data using eqs 3 and 4 provided measurements of the kinetics parameters k_{app} and k_{off}, respectively. Plots of these parameters vs protein concentration showed that k_{app} varied linearly with concentration, while k_{off} stayed constant (Figure 4C). The values extracted for k_{app}, k_{off}, and $1/K_d$ for both Cy5-MBP-His_{11} and Cy5-MBP-His_5 are similar (Table 1), indicating that at pH 7.4 these two proteins self-assemble onto QD surfaces with similar affinity. This is analogous to the general consensus on protein purification with IMAC, where increasing the number of histidine monomers (His_n) beyond six does not improve protein binding or yield.[7,8] However, at pH 9.5, the kinetics of protein self-assembly are drastically changed, with substantially lower binding constant k_{on} and a much larger equilibrium constant $1/K_d$ measured for MBP-His_{11}, while self-assembly of MBP-His_5 was negligible.

Kinetics of QD−Protein/Peptide Self-Assembly in Solution. In these experiments, we kept the protein/peptide-to-QD ratio constant at 1:1 and probed changes in the QD PL loss while varying the overall concentration of reagents in the solution. These conditions ensure that binding events of distinct peptides (or proteins) to a QD are essentially independent. Following mixing, Cy5-labeled proteins progressively self-assemble on the QD surface, resulting in a time-dependent quenching of the QD emission due to FRET interactions between the QD and proximal Cy5 dyes. At low reagent concentrations (below or near K_d^{-1}), when equilibrium is reached, a fraction of Cy5-protein remains free (unbound) in the solution and does not contribute to the QD PL loss. However, as the overall QD and protein concentrations increase, the fraction of bound proteins at equilibrium increases while that of unbound diminishes. Furthermore, the progression toward binding equilibrium depends on the reagents concentration, with faster kinetics anticipated for higher concentration. The time dependence of the QD PL decay thus reflects the kinetics of solution self-assembly (by providing access to k_{app}, k_{on}, and k_{off}), whereas the dependence of the overall relative PL quenching on concentration should provide only information about the equilibrium conditions (K_d^{-1}). We explored self-assembly onto QDs that are capped with either DHLA (short and charge-terminated ligand) or DHLA−PEG1000 (longer neutral ligand). We limited our experiments to using MBP-$His_{5,11}$ and peptide-His_6 as model systems to probe solution-phase self-assembly because most of our previously developed assays employed His_5- and His_6-terminated proteins and peptides;[9,10,13,14] furthermore, previous studies have indicated that longer polyhistidine tags ($n > 6$) do not substantially improve protein binding to Ni−NTA media.[7,23]

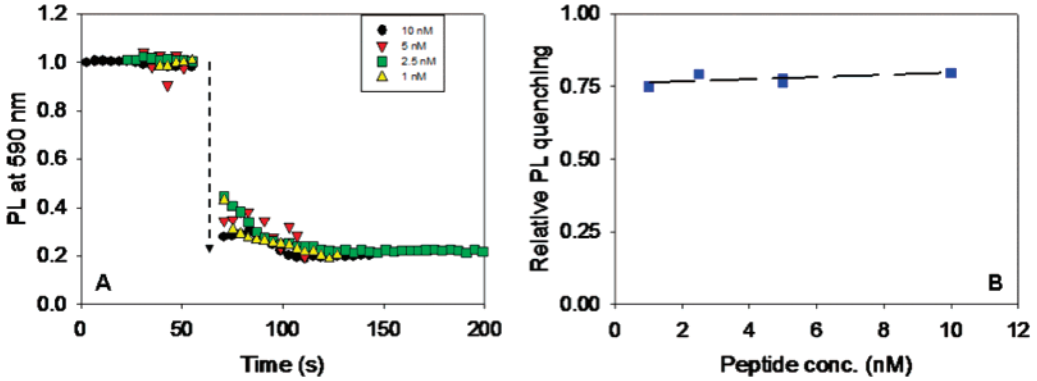

Figure 6. Solution-phase self-assembly on DHLA−PEG1000-capped QDs. (A) Relative PL quenching with time of 590-nm QDs upon binding with Cy5-peptide-His_6 at various peptide concentrations. (B) Relative quenching at equilibrium vs peptide concentration derived from data in (A).

a. Self-Assembly onto DHLA-Capped QDs. Figure 5A illustrates changes in the QD PL with time following mixing of DHLA-capped QDs and Cy5-MBP-His_5; similar data were collected when QDs were mixed with Cy5-peptide-His_6. Data on the time-dependent QD PL decay are easily fit to a monoexponential behavior as predicted by eq 7. For peptide-His_6, k_{on} and k_{off} values were derived from the time-dependent PL loss combined with analysis of the PL quenching at equilibrium for different peptide concentrations (Figure 5B,C and Table 1). However, while the apparent binding rates initially increase with concentration for Cy5-MBP-$His_{5,11}$ (as anticipated from eq 2), they rapidly reach a saturation plateau of 0.02 (for MBP-His_{11}) and 0.04 s^{-1} (for MBP-His_5) at concentrations above ~5 nM (Supporting Information, Figure S-5). The slower self-assembly kinetics at low concentrations allowed us to estimate an upper limit for the dissociation constant of both MBP-$His_{5,11}$ in solution ($k_{off} < 2-3 \times 10^{-3}$ s^{-1}). Figure 5C,D shows that the relative PL quenching at equilibrium reaches a plateau for high reagent concentration, where essentially all proteins/peptides are bound to nanocrystals and contribute to the QD PL quenching. From this concentration-dependent quenching, we derived values for $1/K_d$ for MBP-His_5 and peptide-His_6 using eq 9 (Table 1). In comparison, the relative PL quenching due to self-assembly of Cy5-MBP-His_{11} onto DHLA-capped QDs was constant throughout the concentration range used, which allowed only access to an upper limit of the binding constant (i.e., $K_d^{-1} < 0.5$ nM).

b. Self-Assembly on DHLA−PEG-Capped QDs. Solution-phase experiments performed using Cy5-peptide-His_6 mixed CdSe−ZnS QDs capped with DHLA−PEG1000 (neutral and longer ligand) also showed time-dependent QD PL quenching, indicative of kinetic interactions and binding, but saturation in the PL quenching was very rapidly reached; the experimental setup did not permit higher time resolution near the origin immediately following mixing (Figure 6A). Furthermore, the relative PL quenching for these solution studies was essentially constant throughout the range of reagent concentration used (Figure 6B), similar to the results measured for the self-assembly of DHLA-capped QDs and Cy5-MBP-His_{11} mentioned above. Here, too, we were able to only extract an upper limit for the binding constant ($1/K_d < 0.5$ nM). In comparison, experiments using Cy5-MBP-His_5 and Cy5-MBP-His_{11} mixed with DHLA−PEG1000-capped QDs did not show measurable PL quenching (beyond those expected from solution-phase interactions). This clearly indicates absence of self-assembly between MBP-His_n and DHLA−PEG1000-capped QDs. Lack of self-assembly of MBP-His onto DHLA−PEG-capped QDs was also confirmed using a shorter PEG600-appended DHLA ligand.

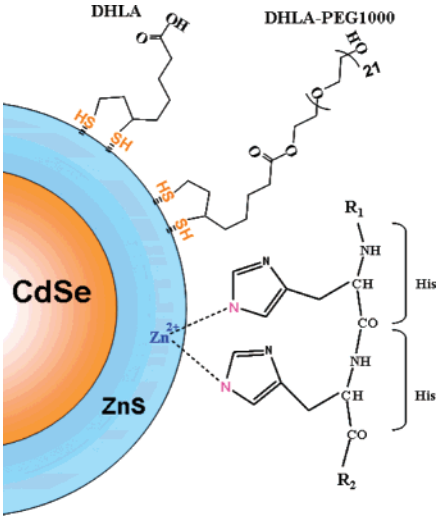

Figure 7. Schematic representation of the metal-affinity interactions and binding stipulated from the experimental data, with coordination of the histidine molecules to Zn on the QD surface. Structure of the DHLA and DHLA−PEG1000 capping ligand is also shown. R_1 and R_2 designate peptide sequence and the terminal Ac amino acid, respectively. Only two His groups are shown for simplicity.

Discussion

In combination, these results provide a few unique insights into understanding what controls metal-affinity driven self-assembly between His-appended proteins and peptides and CdSe−ZnS core−shell QDs. Data show that aspects such as bioreceptor size (peptides vs proteins), length of the His tag, configuration used (surface vs solution-phase self-assembly), and pH conditions affect/influence QD−protein and QD−peptide self-assembly. These experiments combined indicate that self-assembly is driven by direct interactions between the His tag and the metallic QD surface and is not dependent on the ligand charge (Figure 7). The self-assembly is, however, strongly affected by the lateral extension of the surface ligands used to promote QD water solubility. We find that for peptides, which tend to have extended conformation due to their small mass, self-assembly can equally take place onto DHLA-capped and DHLA−PEG1000-capped QDs. Peptides also self-assemble onto surface-immobilized as well as on freely diffusing QDs in solution. The strength of the interactions and therefore stability of the QD−peptide conjugates depend on the polyhistidine size, with tags having shorter than four monomers providing slower binding kinetics and larger equilibrium constants $1/K_d$. However, polyhistidine tags longer than His_6 appear to have limited improvement on the self-assembly kinetics, a result that agrees

well with previous work by Hochuli et al., where affinity of a series of His_n-appended proteins for Ni−NTA media was tested.[7] The peptide interaction with either surface-immobilized or solution-dispersed QDs (capped with charged DHLA or neutral DHLA−PEG) is facilitated by its ability to penetrate through long pegylated ligand shells and interact directly with the metal surface. Conversely, proteins with their larger mass and globular conformation are not able to penetrate the DHLA−PEG1000 ligand shell. (A homogeneous DHLA−PEG1000 shell with ∼15 PEG repeat units is thicker than the extension of a full His_{11} tag.) Thus, proteins appended with His_5 or His_{11} tag can only interact with DHLA-capped QDs (nanocrystals functionalized with shorter ligands), as anticipated from our preliminary study in ref 27. In addition, because of their large size protein-His_n experience slower kinetics and higher equilibrium constants in surface self-assembly. Our data also indicate that, in solution, self-assembly is generally governed by faster kinetics than those measured for self-assembly onto surface-immobilized nanocrystals. We attributed this difference to the ability of the nanocrystals and proteins/peptides to freely interact in solution; the main driving factor will be the probability of encounters in the solution, a property that is governed by the QD and protein/peptide concentrations and diffusion coefficients.

Analysis of the self-assembly data (for DHLA-capped QDs) at different pH's and in either configuration (surface versus solution self-assembly) implies that pH effects on QD-His tag interactions can be more pronounced for proteins than for peptides. We tentatively attribute these differences to pH-dependent net charge of the bioreceptors. Using the protein calculator (http://molbiol-tools.ca), we estimate that MBP-$His_{5,11}$ have a charge of ∼−4 at pH 7.4 which increases to ∼−18 at pH 9.5. In comparison, peptide-His_{4-8} series are only slightly positively charged at pH 7.4, ∼0.5, but become negative ∼−2 at pH 9.5 (Table 1). This overall larger net charge of MBP will likely affect the kinetics of its interactions with and self-assembly on the DHLA-capped QDs. Furthermore, those effects will be more pronounced in surface self-assembly under flow than for solution-phase self-assembly because of higher charge surface density. Additional investigations using self-assemblies of His-terminated biomolecules onto QDs and other metallic nanoparticles in various pH conditions are needed to reach a better understanding of these effects. For example, it would be useful and informative to perform similar binding experiments using peptides that have net positive charges to both DHLA- and DHLA−PEG-capped CdSe−ZnS QDs. Such experiments could provide information on the potential contributions from electrostatic interactions to the binding and its kinetics.

Finally, with $1/K_d$ in the nanomolar range our data indicate that interactions of our QDs with His-terminated proteins and peptides are stronger than most antibody−antigen interactions ($1/K_d \approx 1-1000$ nM).[23] The strong affinity is primarily due to the linear arrangement of several histidine residues that provide polyvalency and cooperative interactions with the nanoparticle surface.[23] The ease with which polyhistidine residues can be appended onto cloned proteins,[40] or incorporated into nascent peptides,[28] makes metal-affinity driven protein/peptide self-assembly an attractive approach to create a wide range of hybrid bioconjugates. A variety of commercial plasmids have been developed to facilitate polyhistidine incorporation onto cloned proteins.[40] Metal-His affinity is stable under various conditions including 1 M NaCl, 1% detergent, certain organic solvents, 30% glycerol and ethanol, up to 10 mM β-mercaptoethanol, and highly denaturing conditions such as 8 M urea and 6 M guanidinium.[23] The polyhistidine motif is known to exhibit a strong affinity to a variety of metals including Ni^{2+}, Cu^{2+}, Co^{2+}, Zn^{2+}, Mn^{2+}, Fe^{2+}, and Cr^{2+}.[23,41,42] These results will have important implications for other nanoparticles that present metallic surfaces with strong affinity to histidine molecules. The present conjugation strategy has not been realized with commercial QDs, presumably because of a thicker solubilizing capping layer; these are usually made of block copolymers (such as a mixture of poly(ethylene glycol) phosphatidylethanolamine (PEG−PE) diblock), which prevent access to the metal-rich surface of the inorganic core.

Conclusion

We have presented a detailed characterization of the kinetics that govern various aspects of metal-affinity driven self-assembly between hydrophilic CdSe−ZnS core−shell luminescent QDs and a series of engineered peptides and proteins appended with polyhistidine tracts at their C- or N-termini. In particular, we explored effects of varying the His tag length, the solution pH, the nature of the solubilizing ligand layer on the QD surface, and the geometry/configuration used to test the self-assembly (near a substrate versus floating in solution). Our data clearly showed that binding is strong with typical equilibrium constant $K_d^{-1} \approx 0.1-100$ nM, and kinetics of binding is fast (e.g., equilibrium is reached at ∼100−200 s in solution). It also confirmed that the strength of the binding depends on the His tag length, but only for tags having less than four monomer units.

Commonly accepted/desired criteria for an "ideal" conjugation strategy include ease of use (reduced preparation and purification steps), versatility (ability to assemble several types of biological molecules onto QDs with high affinity), and preservation of the attached biomolecules subsequent functions. Several of these conditions are satisfied by the metal-affinity driven self-assembly. Furthermore, this technique takes advantage of the ubiquitous use of protein His-tagging as a tool for purification using affinity chromatography. Our data also show that direct access to the metallic surface of the QD is necessary for self-assembly. It will be beneficial if proteins were engineered with an additional spacer inserted between the C- or N-terminus and the polyhistidine tract and tested for tight binding to QDs capped with neutral DHLA−PEG ligands, where stability over a broad pH range is satisfied.

Acknowledgment. The authors acknowledge NRL and the Office of Naval Research (ONR Grant No. N001404WX20270) and Stephen Lee and Ilya Elashvilli at the CB Directorate/Physical S & T Division, DTRA, for support. T.P. acknowledges a postdoctoral fellowship from the Foundation pour la Recherche Medicale (France). S.H. is pleased to acknowledge the generous support of the Office for Research of the University at Albany.

Supporting Information Available: Additional details on peptide synthesis and purification. This material is available free of charge via the Internet at http://pubs.acs.org.

References and Notes

(1) Michalet, X.; Pinaud, F. F.; Bentolila, L. A.; Tsay, J. M.; Doose, S.; Li, J. J.; Sundaresan, G.; Wu, A. M.; Gambhir, S. S.; Weiss, S. *Science* **2005**, *307*, 538.

(2) Medintz, I.; Uyeda, H.; Goldman, E.; Mattoussi, H. *Nat. Mater.* **2005**, *4*, 435.

(3) Kim, S.; Lim, Y. T.; Soltesz, E. G.; De Grand, A. M.; Lee, J.; Nakayama, A.; Parker, J. A.; Mihaljevic, T.; Laurence, R. G.; Dor, D. M.; Cohn, L. H.; Bawendi, M. G.; Frangioni, J. V. *Nat. Biotechnol.* **2004**, *22*, 93.

(4) Alivisatos, A. P.; Gu, W.; Larabell, C. A. *Annu. Rev. Biomed. Eng.* **2005**, *7*, 55.

(5) Parak, W. J.; Pellegrino, T.; Plank, C. *Nanotechnology* **2005**, *16*, R9.
(6) Mattoussi, H.; Mauro, J. M.; Goldman, E. R.; Anderson, G. P.; Sundar, V. C.; Mikulec, F. V.; Bawendi, M. G. *J. Am. Chem. Soc.* **2000**, *122*, 12142.
(7) Hochuli, E.; Bannwarth, W.; Dobeli, H.; Gentz, R.; Stuber, D. *Biotechnology* **1988**, *6*, 1321.
(8) Schmitt, J.; Hess, H.; Stunnenberg, H. G. *Mol. Biol. Rep.* **1993**, *18*, 223.
(9) Clapp, A. R.; Medintz, I. L.; Mauro, J. M.; Fisher, B. R.; Bawendi, M. G.; Mattoussi, H. *J. Am. Chem. Soc.* **2004**, *126*, 301.
(10) Medintz, I. L.; Clapp, A. R.; Mattoussi, H.; Goldman, E. R.; Fisher, B.; Mauro, J. M. *Nat. Mater.* **2003**, *2*, 630.
(11) Goldman, E.; Medintz, I.; Whitley, J.; Hayhurst, A.; Clapp, A.; Uyeda, H.; Deschamps, J.; Lassman, M.; Mattoussi, H. *J. Am. Chem. Soc.* **2005**, *127*, 6744.
(12) Medintz, I. L.; Konnert, J. H.; Clapp, A. R.; Stanish, I.; Twigg, M. E.; Mattoussi, H.; Mauro, J. M.; Deschamps, J. R. *Proc. Natl. Acad. Sci. U.S.A.* **2004**, *101*, 9612.
(13) Medintz, I. L.; Clapp, A. R.; Brunel, F. M.; Tiefenbrunn, T.; Uyeda, H. T.; Chang, E. L.; Deschamps, J. R.; Dawson, P. E.; Mattoussi, H. *Nat. Mater.* **2006**, *5*, 581.
(14) Anikeeva, N.; Lebedeva, T.; Clapp, A. R.; Goldman, E. R.; Dustin, M. L.; Mattoussi, H.; Sykulev, Y. *Proc. Natl. Acad. Sci. U.S.A.* **2006**, *103*, 16846.
(15) Sandros, M. G.; Gao, D.; Benson, D. E. *J. Am. Chem. Soc.* **2005**, *127*, 12198.
(16) Ipe, B. I.; Lehnig, M.; Niemeyer, C. M. *Small* **2005**, *1*, 706.
(17) Ding, S. Y.; Xu, Q.; Ali, M. K.; Baker, J. O.; Bayer, E. A.; Barak, Y.; Lamed, R.; Sugiyama, J.; Rumbles, G.; Himmel, M. E. *BioTechniques* **2006**, *41*, 435.
(18) Lao, U. L.; Mulchandani, A.; Chen, W. *J. Am. Chem. Soc.* **2006**, *128*, 14756.
(19) Zhou, M.; Ghosh, I. *Biopolymers* **2007**, *88*, 325.
(20) Delehanty, J. B.; Medintz, I. L.; Pons, T.; Brunel, F. M.; Dawson, P. E.; Mattoussi, H. *Bioconjugate Chem.* **2006**, *17*, 920.
(21) Goldman, E. R.; Medintz, I. L.; Hayhurst, A.; Anderson, G. P.; Mauro, J. M.; Iverson, B. L.; Georgiou, G.; Mattoussi, H. *Anal. Chim. Acta* **2005**, *534*, 63.
(22) Ipe, B. I.; Niemeyer, C. M. *Angew. Chem., Int. Ed.* **2006**, *45*, 504.
(23) Hainfeld, J. F.; Liu, W.; Halsey, C. M. R.; Freimuth, P.; Powell, R. D. *J. Struct. Biol.* **1999**, *127*, 185.
(24) Dabbousi, B. O.; Rodriguez-Viejo, J.; Mikulec, F. V.; Heine, J. R.; Mattoussi, H.; Ober, R.; Jensen, K. F.; Bawendi, M. G. *J. Phys. Chem. B* **1997**, *101*, 9463.
(25) Hines, M. A.; Guyot-Sionnest, P. *J. Phys. Chem.* **1996**, *100*, 468.
(26) Peng, Z. A.; Peng, X. *J. Am. Chem. Soc.* **2001**, *123*, 183.
(27) Uyeda, H. T.; Medintz, I. L.; Jaiswal, J. K.; Simon, S. M.; Mattoussi, H. *J. Am. Chem. Soc.* **2005**, *127*, 3870.
(28) Schnolzer, M.; Alewood, P.; Jones, A.; Alewood, D.; Kent, S. B. *Int. J. Pept. Protein Res.* **1992**, *40*, 180.
(29) Medintz, I. L.; Goldman, E. R.; Lassman, M. E.; Mauro, J. M. *Bioconjugate Chem.* **2003**, *14*, 909.
(30) Medintz, I. L.; Sapsford, K. E.; Clapp, A. R.; Pons, T.; Higashiya, S.; Welch, J. T.; Mattoussi, H. *J. Phys. Chem. B* **2006**, *110*, 10683.
(31) Sapsford, K. E.; Medintz, I. L.; Golden, J. P.; Deschamps, J. R.; Uyeda, H. T.; Mattoussi, H. *Langmuir* **2004**, *20*, 7720.
(32) Sapsford, K. E.; Liron, Z.; Shubin, Y. S.; Ligler, F. S. *Anal. Chem.* **2001**, *73*, 5518.
(33) Lakowicz, J. R. *Principles of Fluorescence Spectroscopy,* 3rd ed.; Springer: New York, 2006.
(34) Vijayendran, R. A.; Ligler, F. S.; Leckband, D. E. *Anal. Chem.* **1999**, *71*, 5405.
(35) Grimmett, G.; Stirzaker, D. *Probability and Random Processes,* 2nd ed.; Oxford University Press: Oxford, 1992.
(36) Pons, T.; Medintz, I. L.; Wang, X.; English, D. S.; Mattoussi, H. *J. Am. Chem. Soc.* **2006**, *128*, 15324.
(37) Lednev, I. K.; Ermolenkov, V. V.; Higashiya, S.; Popova, N. I.; Topilina, N. I.; Welch, J. T. *Biophys. J.* **2006**, *91*, 3805.
(38) *Bioconjugate Techniques;* Hermanson, G. T., Ed.; Academic Press: San Diego, CA, 1996.
(39) Ueda, E. K. M.; Gout, P. W.; Morganti, L. *J. Chromatogr., A* **2003**, *988*, 1.
(40) Drees, J.; Smith, J.; Schafer, F.; Steinert, K. *Methods Mol. Med.* **2004**, *94*, 179.
(41) Daniel, M. C.; Astruc, D. *Chem. Rev.* **2004**, *104*, 293.
(42) Niemeyer, C. M. *Angew. Chem., Int. Ed.* **2001**, *40*, 4128.